Letter Vol. 42, No. 23 / December 1 2017 / Optics Letters 4865

Optics Letters

Third-order nonlinearity OPO: Schmidt mode decomposition and tripartite entanglement

C. González-Arciniegas,[1,*] Nicolas Treps,[2] and P. Nussenzveig[1]

[1]Instituto de Física, Universidade de São Paulo, São Paulo, 05315-970 São Paulo, Brazil
[2]Laboratoire Kastler Brossel, UPMC-Sorbonne Universités, ENS-PSL Research University, Collége de France, CNRS; 4 place Jussieu, F-75252 Paris, France
*Corresponding author: carlosgonza@usp.br

Received 4 September 2017; revised 11 October 2017; accepted 16 October 2017; posted 17 October 2017 (Doc. ID 306089); published 22 November 2017

We investigate quantum properties of light in optical parametric oscillators (OPOs) based on four-wave mixing gain in media with third-order nonlinearities. In spite of other competing $\chi^{(3)}$ effects such as phase modulation, bipartite and tripartite entanglement is predicted above threshold. These findings are relevant for recent implementations of complementary metal-oxide-semiconductor (CMOS)-compatible on-chip OPOs.

OCIS codes: (270.0270) Quantum optics; (190.4970) Parametric oscillators and amplifiers.

https://doi.org/10.1364/OL.42.004865

Optical parametric oscillators (OPOs) are ubiquitous sources of nonclassical light. Typically, they are based on parametric downconversion (PDC) inside a cavity, a second-order nonlinear process in which pairs of (signal and idler) photons are created upon annihilation of incident pump photons. Owing to energy conservation and phase matching, signal and idler fields have strong intensity correlations and phase anti-correlations, resulting in Einstein–Podolsky–Rosen (EPR)-like entangled states [1]. Entanglement is a coveted resource in quantum information science, and the OPO has been a driver for many advances such as the deterministic teleportation of coherent states [2], the generation of multicolor entanglement [3,4] with potential use for quantum networks [5], and the generation of continuous-variable (CV) cluster states in the time domain [6,7] as well as in the frequency domain [8,9]. The CV entangled states are deterministically generated at a rate which is limited by the OPO cavity bandwidth.

Recent progress in silicon photonics technologies opened a new avenue for on-chip CV quantum information. The ultrasmall footprint of these devices entails large cavity bandwidths and, thus, high repetition rates for quantum communications applications. Indeed, silicon-based micro-cavities have high quality factors ($Q \gtrsim 10^6$), are complementary metal-oxide-semiconductor (CMOS)-compatible, and are also easily connected to commercial fibers. However, second-order nonlinearities are precluded by the material's symmetry properties, and the strongest nonlinearities are of the third order. Four-wave mixing (FWM) can replace PDC as a source of pairs of signal and idler photons, upon annihilation of pairs of pump photons. Several experiments on quantum states of light have been performed using FWM such as the first experimental demonstration of squeezed states [10] and, more recently, the generation of CV entangled states [11] among others. Quantum properties of these on-chip devices have started to be tested and the first experimental generation of squeezed states was recently reported [12]. The generation of frequency combs in this platform [13] also opens the possibility to have a scalable generator of cluster states for applications to CV one-way quantum information [14].

In this Letter, we present a theoretical analysis of $\chi^{(3)}$ OPOs, operating above threshold, with parameters chosen according to current experiments. When limiting to only three excited cavity modes, we predict bipartite and tripartite entanglement, even when including phase modulation effects which are of the same order of the FWM process.

The three cavity modes, named pump, signal, and idler, have resonant frequencies ω_p, ω_s, and ω_i, respectively. Each mode is described by a corresponding annihilation operator $\hat{a}$. The Hamiltonian, in the rotating wave approximation, is given by

$$\hat{H} = \hat{H}_0 + \hat{H}_{\text{int}},$$

where the free Hamiltonian $\hat{H}_0$ is given by

$$\hat{H}_0 = \hbar \sum_{j=\{p,s,i\}} \omega_j \hat{a}_j^\dagger \hat{a}_j.$$

Owing to the dispersion in the cavity, resulting from the geometry and the material dispersion, the mode resonances, in general, are not equally spaced. We define the parameter $D_3 = 2\omega_p - \omega_s - \omega_i$ to quantify this dispersion. This quantity can be easily engineered in the context of silicon (or silicon-nitride)-based ring micro-cavities by modifying the radius and/or the transversal shape of the ring.

The nonlinear interaction Hamiltonian $\hat{H}_{\text{int}}$ is given by

$$\hat{H}_{\text{int}} = -\hbar\eta \Big[\frac{1}{2}(\hat{a}_p^\dagger \hat{a}_p^\dagger \hat{a}_p \hat{a}_p + \hat{a}_s^\dagger \hat{a}_s^\dagger \hat{a}_s \hat{a}_s + \hat{a}_i^\dagger \hat{a}_i^\dagger \hat{a}_i \hat{a}_i) + 2(\hat{a}_p^\dagger \hat{a}_s^\dagger \hat{a}_p \hat{a}_s + \hat{a}_p^\dagger \hat{a}_i^\dagger \hat{a}_p \hat{a}_i + \hat{a}_s^\dagger \hat{a}_i^\dagger \hat{a}_s \hat{a}_i) + (\hat{a}_s^\dagger \hat{a}_i^\dagger \hat{a}_p \hat{a}_p + \hat{a}_p^\dagger \hat{a}_p^\dagger \hat{a}_s \hat{a}_i)\Big].$$

Here η is proportional to the $\chi^{(3)}$ coefficient. The first and second terms in $\hat{H}_{\rm int}$, respectively, are the self- and cross-phase modulation (SPM and XPM) terms, and they are responsible for intensity dependent shifts of the resonant frequencies. The last term is the FWM term which is responsible for the energy exchange between the three modes. The SPM and XPM terms play important roles in the oscillation process and in the noise and entanglement properties of the system.

This Hamiltonian, together with the nonunitary evolution related with losses and the incoming coupled fields into the cavity (vacuum for the signal and idler and a coherent state of frequency Ω_p for the pump), leads to the following Heisenberg–Langevin equations for the annihilation operators:

$$\begin{aligned}\frac{d\hat{a}_p}{dt} &= -(\Gamma_p + i\Delta_p)\hat{a}_p + i\eta[(\hat{a}_p^\dagger\hat{a}_p + 2\hat{a}_s^\dagger\hat{a}_s + 2\hat{a}_i^\dagger\hat{a}_i)\hat{a}_p + 2\hat{a}_p^\dagger\hat{a}_s\hat{a}_i] \\ &\quad + \sqrt{2\gamma_p}\hat{a}_p^{\rm in} + \sqrt{2\mu_p}\hat{a}_p^{\rm loss}, \\ \frac{d\hat{a}_s}{dt} &= -(\Gamma_s + i\Delta_s)\hat{a}_s + i\eta[(2\hat{a}_p^\dagger\hat{a}_p + \hat{a}_s^\dagger\hat{a}_s + 2\hat{a}_i^\dagger\hat{a}_i)\hat{a}_s + \hat{a}_p^2\hat{a}_i^\dagger] \\ &\quad + \sqrt{2\gamma_s}\hat{a}_s^{\rm in} + \sqrt{2\mu_s}\hat{a}_s^{\rm loss}, \\ \frac{d\hat{a}_i}{dt} &= -(\Gamma_i + i\Delta_i)\hat{a}_i + i\eta[(2\hat{a}_p^\dagger\hat{a}_p + 2\hat{a}_s^\dagger\hat{a}_s + \hat{a}_i^\dagger\hat{a}_i)\hat{a}_i + \hat{a}_p^2\hat{a}_s^\dagger] \\ &\quad + \sqrt{2\gamma_i}\hat{a}_i^{\rm in} + \sqrt{2\mu_i}\hat{a}_i^{\rm loss}, \end{aligned} \tag{1}$$

where we have replaced operators $\hat{a}_j$ for corresponding slowly varying operators $\hat{a}_j \to \hat{a}_j e^{-i\Omega_j t}$; $j = p, s, i$. The Ω_j are the carrier frequencies that fulfill energy conservation $2\Omega_p - \Omega_s - \Omega_i = 0$. The terms $\Delta_j \equiv \omega_j - \Omega_j$ are the field detunings relative to the cavity resonances that fulfill $D_3 = 2\Delta_p - \Delta_s - \Delta_i$. The quantities γ_j and μ_j represent the rates for the cavity coupling to output modes and for other losses (scattering, absorption etc.). Total losses are given by $\Gamma_j = \gamma_j + \mu_j$. As long as the cavity modes have similar field profiles, we can set $\Gamma_p = \Gamma_s = \Gamma_i = \Gamma$ (likewise for γ_j and μ_j). The operators $\hat{a}^{\rm in}$ and $\hat{a}^{\rm loss}$ correspond to the annihilation operators for incoming and loss modes of the cavity that have zero mean value, except for the incoming pump ($\langle\hat{a}_p^{\rm in}(t)\rangle = \sqrt{P_{\rm in}/(\hbar\Omega_p)}$), and their fluctuations are delta-correlated $\langle\delta\hat{a}_j^{\rm loss/in\dagger}(t)\delta\hat{a}_k^{\rm loss/in}(t')\rangle = \delta_{j,k}\delta(t-t')$. Finally, we have that the incoming, intra-cavity and output fields are related by the usual beam splitter relation $\hat{a}^{\rm out} = -\hat{a}^{\rm in} + \sqrt{2\gamma}\hat{a}$.

We proceed by linearizing the quantum fluctuations, $\hat{a} = \alpha + \delta\hat{a}$. The mean values $\langle\hat{a}_j\rangle = \alpha_j$ satisfy the classical equations corresponding to the substitution $\hat{a} \to \alpha$ in (1). Following Ref. [15], we solve these classical equations in the steady state by setting $\alpha_j = A_j e^{i\theta_j}$ and accounting for the real and imaginary parts. Two coupled algebraic equations for the amplitudes $A = A_s = A_i$ and A_p are obtained in terms of the experimentally adjustable parameters, the normalized input pump power $F^2 = \frac{2\gamma_p\eta}{\hbar\Omega_p\Gamma^3}P_{\rm in}$, and detuning Δ_p (where $\Delta_s = \Delta_i$):

$$\begin{aligned} A_p^4 &= 1 + \left(\Delta_p - \frac{D_3}{2} - 2A_p^2 - 3A^2\right)^2 \\ F^2 &= A_p^2\left\{\left(1 + \frac{2A^2}{A_p^2}\right)^2 + \left[\Delta_p - A_p^2 - \frac{2A^2}{A_p^2}\left(\Delta_p - \frac{D_3}{2} - 3A^2\right)\right]^2\right\}. \end{aligned} \tag{2}$$

We work with normalized quantities replacing $A \to \sqrt{\frac{\eta}{\Gamma}}A$; $D_3 \to D_3\Gamma$; $\Delta_p \to \Delta_p\Gamma$. The numerical solutions for (2), in the case of perfect frequency matching ($D_3 = 0$) for different values of pump detuning Δ_p are shown in Figs. 1(a) and 1(b), while the case of perfect pump resonance ($\Delta_p = 0$) for several values of D_3 is plotted in Figs. 1(c) and 1(d). On the left (a, c) we have the intracavity pump power A_p^2 and on the right (b, d) the signal and idler power A^2.

Consequences of phase modulation are evident in Fig. 1. For instance, the intracavity pump field does not have a constant value above threshold, in contrast to the $\chi^{(2)}$ scenario [16], depending instead on the incoming power. Exactly on resonance and for perfect frequency matching [Figs. 1(a) and 1(b)], there is no oscillation. This is because when we increase the pump power in order to trigger the oscillation, the phase modulation shifts the mode frequencies out of resonance. It is necessary to pump the resonator with nonzero detuning (even larger than the cavity linewidth) to compensate for this effect. In the case of perfect resonance, this compensation is done by the frequency mismatch [Figs. 1(c) and 1(d)]. For the same reason, our model predicts that for higher values of F^2 the oscillation ceases. In most experiments, however, higher pump powers excite other cavity modes, leading to the generation of frequency combs. This feature is not predicted in the model, given that only three modes are taken into account.

Noise properties are calculated by writing (1) up to first order in quantum fluctuations $\delta\hat{a}_i$. Defining a vector of fluctuations as

$$\delta\hat{\mathbf{A}} = \{\delta\hat{a}_p e^{-i\theta_p}, \delta\hat{a}_p^\dagger e^{i\theta_p}, \delta\hat{a}_s e^{-i\theta_s}, \delta\hat{a}_s^\dagger e^{-i\theta_s}, \delta\hat{a}_i e^{-i\theta_i}, \delta\hat{a}_i^\dagger e^{-i\theta_i}\}^T,$$

where θ_i is the mean field phase $\alpha_i = A_i e^{i\theta_i}$, the evolution of these fluctuations is given by

$$\begin{aligned} \frac{d\delta\hat{\mathbf{A}}}{d\tau} &= -\mathbb{M}_a\cdot\delta\hat{\mathbf{A}} + \frac{\mathbb{T}_a^{\rm in}}{\Gamma}\cdot\delta\hat{\mathbf{A}}^{\rm in} + \frac{\mathbb{T}_a^{\rm loss}}{\Gamma}\cdot\delta\hat{\mathbf{A}}^{\rm loss} \\ \mathbb{T}_a^{\rm in} &= {\rm Diag}\left\{\sqrt{2\gamma_p}e^{-i\theta_p}, \sqrt{2\gamma_p}e^{i\theta_p}, \sqrt{2\gamma}, \sqrt{2\gamma}, \sqrt{2\gamma}, \sqrt{2\gamma}\right\}, \end{aligned} \tag{3}$$

with $\mathbb{T}_a^{\rm loss}$ defined in the same way as $\mathbb{T}_a^{\rm in}$, but changing γ by μ and where $\tau = t\Gamma$ is the normalized time. The matrix $\mathbb{M}_a$ is derived from the linearization process, and its elements are functions of the field's mean values and the detunings.

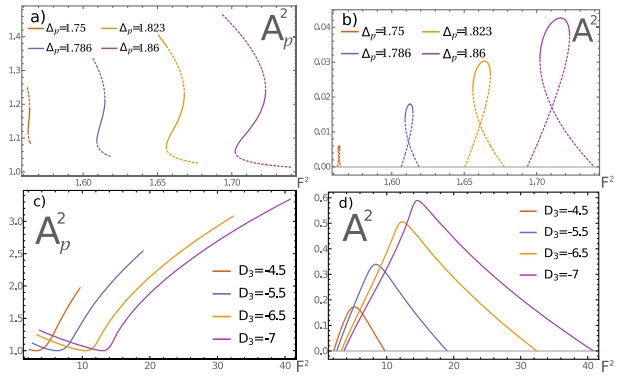

Fig. 1. Intracavity pump (left) and signal-idler (right) amplitudes for several values of pump detuning Δ_p at perfect frequency matching $D_3 = 0$ (top) and on resonance with the pump, $\Delta_p = 0$ for several values of frequency matching D_3 (bottom). The dashed lines represent unstable solutions.

As a first step, we treat the pump classically ($\delta\hat{a}_p \to 0$) and study only the signal-idler correlations. The observables of interest are the quadrature operators of each field $\hat{x} = (\hat{a} + \hat{a}^\dagger)/\sqrt{2}$ and $\hat{y} = -i(\hat{a} - \hat{a}^\dagger)/\sqrt{2}$, referred to as intensity and phase quadratures, respectively, which satisfy the commutation relation $[\hat{x}, \hat{y}] = i$.

Equation (3) decouples if we write it in the sum/subtraction basis. Thus, the vector $\delta\hat{\mathbf{X}}_{pm} = \{\delta\hat{y}_+, \delta\hat{x}_+, \delta\hat{y}_-, \delta\hat{x}_-\}^T$, with $\hat{x}_\pm = (\hat{x}_s \pm \hat{x}_i)/\sqrt{2}$ and $\hat{y}_\pm = (\hat{y}_s \pm \hat{y}_i)/\sqrt{2}$, fulfills the equation

$$\frac{d\delta\hat{\mathbf{X}}_{pm}}{d\tau} = \mathbb{M}_{pm}\cdot\delta\hat{\mathbf{X}}_{pm} + \frac{\mathbb{T}^{\text{in}}_{pm}}{\Gamma}\cdot\delta\hat{\mathbf{X}}^{\text{in}}_{pm} + \frac{\mathbb{T}^{\text{loss}}_{pm}}{\Gamma}\cdot\delta\hat{\mathbf{X}}^{\text{loss}}_{pm}$$
$$\mathbb{M}_{pm} = \text{diag}\{\mathbb{M}_+, \mathbb{M}_-\}, \tag{4}$$

where $\mathbb{M}_+$ and $\mathbb{M}_-$ are 2×2 matrices. Next, we calculate the noise spectral density matrix $S(\omega)$ as $S(\omega)\delta(\omega+\omega') = \langle\delta\hat{X}_{pm}(\omega)\delta\hat{X}_{pm}(\omega')^T\rangle$ from which we can extract all the noise and entanglement information. In particular, we can evaluate the Duan inequality [17] to test signal-idler entanglement:

$$\Delta^2\hat{x}_- + \Delta^2\hat{y}_+ - 1 \geq 0. \tag{5}$$

The inequality (5) is presented in Fig. 2 for different values of D_3 as a function of F^2. Negative values of this quantity (i.e., violation of Duan inequality) imply entanglement between signal and idler. Entanglement detected using (5) is highly limited to a small region for high values of F^2. Here, typical experimental parameters were used, $\omega/\Gamma = 1.5\times 10^{-2}$ and $\gamma/\Gamma = 0.55$, which correspond to an analysis frequency of 3 MHz, a bandwidth of 200 MHz, intrinsic and loaded Qs of 10^6 and 450.000, respectively, for $\lambda_p = 1561$ nm.

In contrast to PDC-based OPOs, where the Duan inequality has been proven as an excellent entanglement witness, we observe the effects of phase modulation here. As pointed out by Ferrini *et al.* [18], the phase modulation distorts the noise ellipse and, thus, the strongest correlations are not between the difference of intensities $\hat{x}_-$ and the sum of the *phases* $\hat{y}_+$. Stronger correlations exist among other quadratures to be determined.

We proceed by calculating the Schmidt modes, which provide the best attainable squeezing for the system [18]. The Schmidt modes quadratures (denoted with the superscript *rot*) are given by a *rotation* of the quadratures in the following way:

$$\begin{pmatrix} y^{rot}_\pm \\ x^{rot}_\pm \end{pmatrix} = \begin{pmatrix} \cos(\theta_\pm) & \sin(\theta_\pm) \\ -\sin(\theta_\pm) & \cos(\theta_\pm) \end{pmatrix}\begin{pmatrix} y_\pm \\ x_\pm \end{pmatrix}, \tag{6}$$

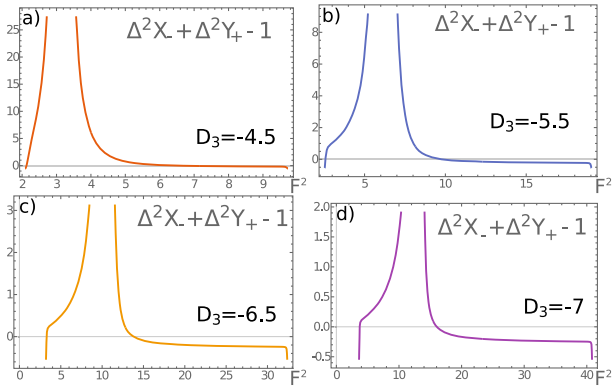

Fig. 2. Left-hand side of Duan inequality (5) for $\Delta_p = 0$ and different values of D_3. Negative value signal entanglement in the system.

such that the noise spectral density matrix is diagonal. The Duan inequality for testing signal-idler entanglement using the rotated quadratures can be rewritten in terms of the Schmidt mode quadratures as [19]

$$\Delta^2\hat{x}^{rot}_- + \Delta^2\hat{y}^{rot}_+ - |C| \geq 0 \qquad \text{with } C = \cos(\theta_+ - \theta_-). \tag{7}$$

The modified Duan inequality is displayed in Fig. 3, indicating that the parameter region where entanglement is detected increases appreciablyand only in a small region no entanglement is detected. The rotations for the sum and subtraction quadratures are independent. The subtraction rotation is negligible, $|\theta_-/\pi| < 10^{-5}$, but the rotation of the sum is significant (see Fig. 4), providing a better quadrature to detect entanglement. The regions where the left-hand side of (7) is bigger coinciding with the region of larger rotation of the sum quadrature which is related with the signal-idler intensity maximum, where the phase modulation effects are bigger. In particular, the inequality is not violated for $\theta_+ \approx \pi/2$ where $\hat{y}^{rot}_+ \approx \hat{x}_+$, i.e., only intensity information is considered and, therefore, the inequality must be fulfilled.

Next we analyze the three mode system by taking into account the quantum fluctuations of the pump field. Defining the vector $\delta\hat{\mathbf{X}} = \{\delta\hat{y}_p, \delta\hat{x}_p, \delta\hat{y}_+, \delta\hat{x}_+, \delta\hat{y}_-, \delta\hat{x}_-\}$, its linearized equation of motion is given by

$$\frac{d\delta\hat{\mathbf{X}}}{d\tau} = \mathbb{M}\cdot\delta\hat{\mathbf{X}} + \frac{\mathbb{T}^{\text{in}}}{\Gamma}\cdot\delta\hat{\mathbf{X}}^{\text{in}} + \frac{\mathbb{T}^{\text{loss}}}{\Gamma}\cdot\delta\hat{\mathbf{X}}^{\text{loss}}.$$

In this situation, the pump fluctuations couple only to the sum subspace, while the subtraction remains the same as in the previous case. The $\mathbb{M}$ matrix is block diagonal $\mathbb{M} = \text{diag}\{\mathbb{M}_{p_+}, \mathbb{M}_-\}$, where $\mathbb{M}_{p_+}$ couples the sum and pump modes, and $\mathbb{M}_-$ is the same as in (4) (explicit expressions of these matrices can be found in [20]). In order to analyze tripartite entanglement, we use the van Loock–Furusawa criteria [21]. We resort again to the Schmidt modes to find the linear combination which is best to detect entanglement. Schmidt quadratures $\hat{\boldsymbol{\xi}} = \{\hat{\xi}_1, \hat{\xi}_2, \hat{\xi}_3, \hat{\xi}_4\}^T$ are determined by

$$\hat{\boldsymbol{\xi}} = \mathbb{U}\cdot\hat{\mathbf{X}}_{p_+}, \tag{8}$$

with $\hat{\mathbf{X}}_{p_+} = \{\hat{x}_p, \hat{y}_p, \hat{x}_+, \hat{y}_+\}^T$, and where $\mathbb{U}$ is the Schmidt transformation (unitary) relating the Schmidt modes with the original modes, and diagonalizes the noise spectral density matrix. The Schmidt quadratures of the substraction subspace are the same as in (6). In addition to being of higher dimension, the matrix $\mathbb{U}$ can also be complex and cannot be seen as a geometrical rotation in a four-dimensional space as in the previous

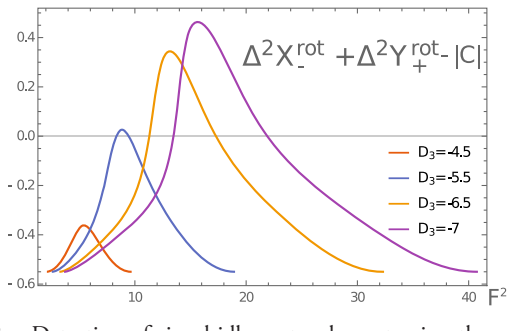

Fig. 3. Detection of signal-idler entanglement using the modified Duan inequality (7), for $\Delta_p = 0$ and several values D_3. Values below 0 indicate entanglement.

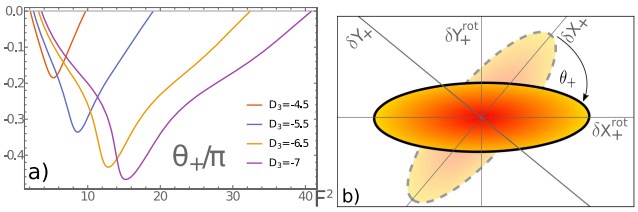

Fig. 4. (a) Rotation angle for the sum subspace as a function of the incoming power with $\Delta_p = 0$ for several values of D_3. (b) Representation of the effect of the quadrature rotation. The noise ellipse axis is aligned with the $\{\delta X_+, \delta Y_+\}$ axis.

case. In terms of the Schmidt quadratures with lower noise, the van Loock–Furusawa inequalities take the form

$$\Delta^2\xi_i + \Delta^2\xi_j - |S_I^{i,j}| \geq 0 \text{ and } \Delta^2 x_-^{rot} + \Delta^2\xi_j - |P_I^j| \geq 0, \quad (9)$$

where $S_I^{i,j}$ and P_I^j are separability constants that depend on the quadratures ξ_i ($i = 3, 4$ the quadratures with less noise) and x_-^{rot} used, the bipartition I in which the inseparability is being tested, and are functions of the matrices in (6) and (8). Since the system is symmetric on the interchange of the signal and idler field, the separability constants are the same for the bipartitions $I_1 = \{s|i,p\}$ and $I_2 = \{i|s,p\}$.

Figures 5 and 6 show the left-hand side of the two inequalities of the form (9) that are violated for the Schmidt quadratures. The violation of the inequality (negative values) plotted in Fig. 5 demonstrates entanglement between the pump mode

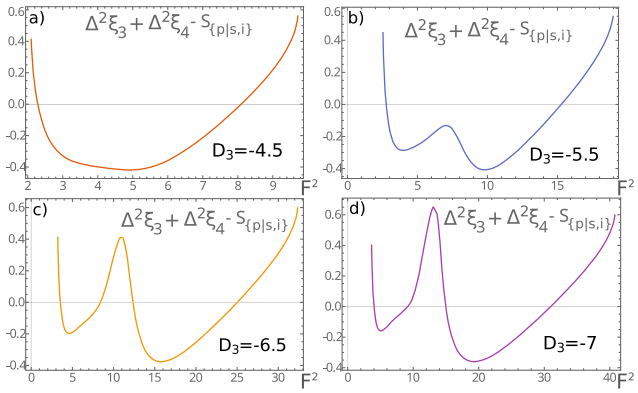

Fig. 5. Inseparability test for partition $I = \{p|s,i\}$.

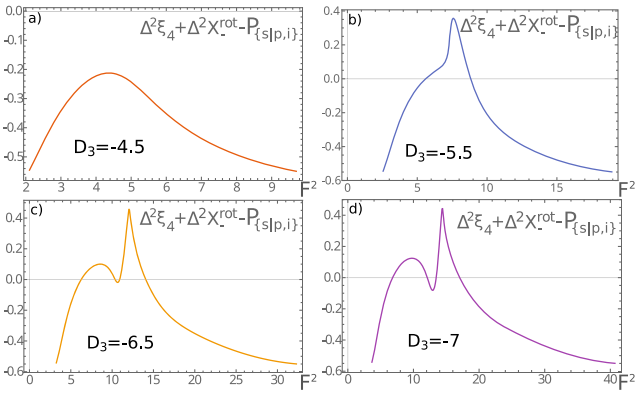

Fig. 6. Inseparability test for partitions $I = \{s|i,p\} = \{i|s,p\}$.

in one side and the signal-idler modes on the other. Given the symmetry of the system, the violation of the inequality plotted in Fig. 6 demonstrates inseparability of the signal from the pump-idler modes, as well as inseparability of the idler from the pump-signal modes.

In summary, we have provided, to the best of our knowledge, the first complete theoretical analysis of three-mode correlations in a $\chi^{(3)}$ OPO operating above threshold, taking into account phase modulation effects, as well as mode dispersion inherent to on-chip realizations. We predict tripartite pump-signal-idler entanglement, as observed in the $\chi^{(2)}$ OPO [3]. On-chip generation of CV multipartite entangled states shall be especially useful for ultra-short distance quantum communications on the scale of future quantum processors.

Funding. Fundação de Amparo à Pesquisa do Estado de São Paulo (FAPESP); Conselho Nacional de Desenvolvimento Científico e Tecnológico (CNPq); Coordenação de Aperfeiçoamento de Pessoal de Nível Superior (CAPES); Institut Universitaire de France (IUF).

Acknowledgment. The authors thank Dr. Avik Dutt, Prof. M. Martinelli, and Prof. Michal Lipson for useful discussions.

REFERENCES

1. M. D. Reid and P. D. Drummond, Phys. Rev. Lett. **60**, 2731 (1988).
2. A. Furusawa, J. Sørensen, S. L. Braunstein, C. A. Fuchs, H. J. Kimble, and E. S. Polzik, Science **282**, 706 (1998).
3. A. S. Coelho, F. A. S. Barbosa, K. N. Cassemiro, A. S. Villar, M. Martinelli, and P. Nussenzveig, Science **326**, 823 (2009).
4. F. A. S. Barbosa, A. S. Coelho, A. J. de Faria, K. N. Cassemiro, A. S. Villar, P. Nussenzveig, and M. Martinelli, Nat. Photonics **4**, 858 (2010).
5. H. J. Kimble, Nature **453**, 1023 (2008).
6. S. Yokoyama, R. Ukai, S. C. Armstrong, C. Sornphiphatphong, T. Kaji, S. Suzuki, J.-I. Yoshikawa, H. Yonezawa, N. C. Menicucci, and A. Furusawa, Nat. Photonics **7**, 982 (2013).
7. X. Su, S. Hao, X. Deng, L. Ma, M. Wang, X. Jia, C. Xie, and K. Peng, Nat. Commun. **4**, 2828 (2013).
8. J. Roslund, R. M. de Araújo, S. Jiang, C. Fabre, and N. Treps, Nat. Photonics **8**, 109 (2013).
9. M. Chen, N. Menicucci, and O. Pfister, Phys. Rev. Lett. **112**, 120505 (2014).
10. R. Slusher, L. Hollberg, and B. Yurke, Phys. Rev. Lett. **55**, 2409 (1985).
11. V. Boyer, A. Marino, R. Pooser, and P. Lett, Science **321**, 544 (2008).
12. A. Dutt, K. Luke, S. Manipatruni, A. L. Gaeta, P. Nussenzveig, and M. Lipson, Phys. Rev. Appl. **3**, 044005 (2015).
13. J. S. Levy, A. Gondarenko, M. A. Foster, A. C. Turner-Foster, A. L. Gaeta, and M. Lipson, Nat. Photonics **4**, 37 (2010).
14. N. C. Menicucci, P. Van Loock, M. Gu, C. Weedbrook, T. C. Ralph, and M. A. Nielsen, Phys. Rev. Lett. **97**, 13 (2006).
15. A. Matsko, A. Savchenkov, D. Strekalov, V. Ilchenko, and L. Maleki, Phys. Rev. A **71**, 033804 (2005).
16. C. Fabre, P. Cohadon, and C. Schwob, Quantum Semiclass. Opt. **9**, 165 (1997).
17. L.-M. Duan, G. Giedke, J. Cirac, and P. Zoller, Phys. Rev. Lett. **84**, 2722 (2000).
18. G. Ferrini, I. Fsaifes, T. Labidi, F. Goldfarb, N. Treps, and F. Bretenaker, J. Opt. Soc. Am. B **31**, 1627 (2014).
19. V. Giovannetti, S. Mancini, D. Vitali, and P. Tombesi, Phys. Rev. A **67**, 022320 (2003).
20. C. Gonzalez Arciniegas, "Properties of the light emitted by a silicon on-chip optical parametric oscillator (OPO)," Ph.D. dissertation (Universidade de São Paulo, 2017).
21. P. van Loock and A. Furusawa, Phys. Rev. A **67**, 052315 (2003).